Monolayers of Apolipoproteins at the Air/Water Interface

Víctor M. Bolaños-García

Department of Biochemistry, University of Cambridge, 80 Tennis Court Road CB2 1GA, Cambridge, England

Salvador Ramos and Rolando Castillo*

Instituto de Física, UNAM. P.O. Box 20-364, D.F., 01000 México

Juan Xicohtencatl-Cortes and Jaime Mas-Oliva

Instituto de Fisiología Celular, P.O. Box 70−243, D.F., 04510 México

Received: February 23, 2001

Human apolipoproteins AII, CIII, E3, and AI were studied from different points of view: secondary structure prediction analysis, protein stability to overcome and revert thermal denaturation, and phase behavior of their monolayer. We found a well-preserved relationship among the predicted secondary structure, amphipatic α-helices, and the ability to recover their secondary protein structure after thermal treatment. With each one of the apolipoproteins studied, the equilibrium character of the unfolding process and the presence of isochromatic points suggested a two-state character for the process. Pressure−area isotherms were carried out, as well as direct observations with a Brewster angle microscope of the apolipoproteins monolayers deposited onto a highly ionic water subphase. We described the gas/liquid-phase transition in all of these proteins. The apolipoproteins AI and AII present a phase transition between two condensed phases at high lateral pressures. A model of the secondary structure for these proteins is presented.

1. Introduction

Langmuir monolayers at the air/water interphase have been thoroughly studied for a long time. However, sensible advances have been obtained just in the past decade, because of new experimental techniques such as X-ray diffraction, polarized fluorescence microscopy, and Brewster angle microscopy (BAM). These new experimental techniques have revealed that most of the singularities in the surface pressure−area isotherms are due to phase changes, where each phase has a different molecular organization. The work of many different groups has contributed to obtain a general picture of the phase diagram of monolayers as well as the structure of their phases.[1]

Several studies have been carried out in protein monolayers made of horse muscle cytochrome,[2−4] acetylcholinesterase,[5] streptavidin,[6] human lung surfactant protein SP-B and its amino terminus ($SP\text{-}B_{1-25}$),[7] tetra-α-helical heme proteins $(\alpha ss\alpha)_2$,[8] and quite recently, a study with the human apoliprotein CI[9] (APO CI) presented by our group. When APO CI was deposited onto a highly ionic water subphase, two first-order phase transitions were found under compression. The first phase transition involved the coexistence of a fluid condensed phase and a gas phase, whereas the second phase transition was a transition between two condensed phases. A protein model was proposed, where APO CI is made of two-amphipathic α-helices bonded with a poorly structured polypeptide fragment. The second phase transition could be explained as a conformational change in the protein. This conformational change has been studied with X-ray diffraction[10] and with atomic force microscopy.[11]

This paper is devoted to the study of the human apolipoproteins (APOs) AII, CIII, E3, and AI. Because these molecules have not been X-ray solved, we present a complete secondary structure prediction analysis. We also present measurements of protein stability to overcome and revert thermal denaturation in different ionic strength conditions. This information helps us to understand the secondary structure predictions made in our study and explore the stability of these apolipoproteins in the different experimental conditions employed. Finally, we consider the monolayer phase behavior of these proteins, as a step toward the understanding of their behavior at interfaces, where their physiological function is important. The outline of the paper is the following: In section 2, a review of the human apolipoproteins is presented. Our experimental procedures are presented in section 3. In section 4, the results and a discussion are presented.

2. Human Apolipoproteins

Apolipoproteins combine with lipids in order to form several classes of lipoprotein particles. Different combinations of lipid and protein produce lipoprotein particles of different density, size, and, therefore, specific functions. APOs AI, AII, AIV, CI, CII, CIII, and E3 are known as exchangeable apolipoproteins because of their capability to move and exchange between lipoproteins.[12] Although this phenomenon has been well documented, the specific mechanisms that govern this behavior are still not well understood.

Human APO AII is a major component of the HDL (high density lipoproteins) particles and it is synthesized mainly in the liver.[13−15] Recent advances with APO AII genetics have suggested that this molecule plays a significant role in HDL

* To whom correspondence should be addressed. E-mail: rolandoc@fenix.fisica.unam.mx.

10.1021/jp010714b CCC: $20.00
Published on Web 06/14/2001

metabolism.[15−17] APO AII has been also shown to be able to displace APO AI from the surface of HDL particles, which in turn might account for its ability to impair reverse cholesterol transport induced by APO AI, therefore, enhancing the risk of atherosclerosis.[15,18] APO CIII contained in HDL particles corresponds up to 60% of its total protein mass.[12,19] Although their entire functions have not been revealed yet, APO CIII has been postulated to be a modulator of the receptor-mediated clearance of lipoproteins.[20,21] APO E3 is a plasma protein that mediates the interaction of APO E3-containing lipoproteins with the LDL (low-density lipoprotein) receptor and the chylomicron remnant APO E3-receptor. In consequence, APO E3 plays a critical role in determining the metabolic fate of several classes of lipoproteins and plays a central role in cholesterol metabolism.[22,23] APO AI is importantly associated to HDL particles.[24] Human APO AI transgenic mice have established that APO AI is responsible for the protective effect of HDL against coronary artery disease.[25−27] APO AI is also a potent activator of the lecithin acyl transferase, enzyme responsible for the formation of most cholesterol esters in plasma.[28−30]

3. Experimental Section

Lyophilized recombinant human apoE3 was kindly provided by Dr. K. H. Weisgraber (Gladstone Institute for Cardiovascular Research, San Francisco, CA). Lyophilized APOs AII, CIII, and AI, isolated from its natural source, were purchased from Sigma Chemical Co. (San Louis, MO). Protein solutions were always filtered using 0.22 μm membrane filters before carrying out the experiments.

The protein concentration was determined according to the equation $A = \epsilon lC$. Here, A is sample absorbance, l is the path length, ϵ is the molar absorption coefficient, and C is the protein concentration. ϵ at 280 nm was obtained according to the procedure described by Pace et al.[31]

Far-UV circular dichroism (CD) spectra were recorded on an Aviv 62DS spectropolarimeter (Aviv 62DS; Aviv Associates Inc., NJ) in a 0.1 cm quartz cell, using an average time of 0.3 s and a step size of 0.5 nm at 20 °C and pH 8.0. The α-helix content was calculated using the program PROSEC 3.1 (Aviv Associates Inc., NJ). These measurements were carried out to evaluate protein stability during either chemical or thermal denaturation as well as to ensure protein integrity before the monolayer preparation. For the heat unfolding studies, the heating rate was 10 °C/h. Five independent curves for each temperature were performed. The average protein concentration employed during these determinations ranged between 150 and 200 μg/mL.

Apolipoproteins were solubilized in a buffered solution and spread onto a subphase of a phosphate buffered solution (20 mM, pH 8.0) prepared with ultrapure water (Nanopure-UV) containing 3.5 M KCl (Baker, Mexico). The different apolipoprotein spreading solutions were diluted to a final concentration ca. 0.2 mg/mL. It is important to note that before preparing the KCl solution the KCl salt was heated for 4 h at 300 °C to prevent spurious organic compounds in the surface of the subphase. Monolayers were prepared on a computerized Nima Langmuir−Blodgett trough (TKB 2410A; Nima Technology Ltd., England) using a Wilhelmy plate to measure the surface pressure, $\Pi = \gamma_0 - \gamma$, i.e., the surface tension difference of the clean subphase and that of the protein covered subphase. The cleanliness of the subphase can be assured making a compression of the barriers without protein and obtaining a negligible pressure rise ($\Pi < 0.1$ mN/m).

The trough was isolated from vibrations using a pneumatic tube incorporated into a steel base. The barriers are made of PTFE fitted with stiffening bars defining a working circular area, starting at 1000 cm^2. All experiments were carried out in a dust-free environment at 25 °C. The temperature in the trough was kept constant at 25 °C with the aid of a water circulation bath. The speed of compression was in the order of 50 cm^2/min. This compression rate corresponds to 145, 145, 462, and 734 Å^2/molec. min for APOs AII, CIII, E3, and AI, respectively.

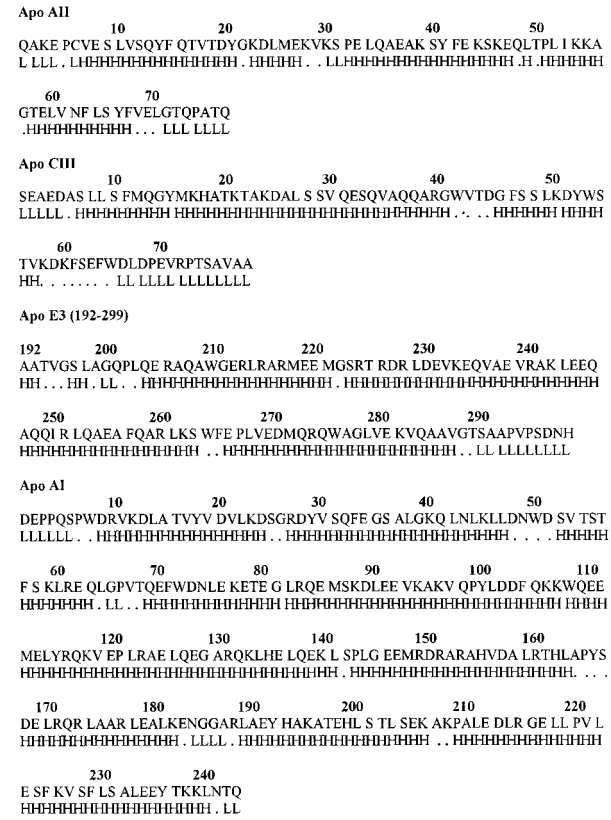

Figure 1. Secondary structure prediction for APO AII, APO CIII, APO E3, and APO AI according to the PHD method. H = α helix, L = loop, and ● = no prediction is made for these amino acid residues.

BAM observations were performed in a BAM1 Plus (Nanofilm Technologie GmbH, Germany), with a spatial resolution ca. 4 μm. Here, the interface is illuminated at the Brewster incidence (∼53°) with a polarized laser beam from a He−Ne laser. A microscope receives the reflected beam that is analyzed by a polarization analyzer, and the signal is received by a CCD video camera to develop an image of the monolayer.

For secondary structure predictions, the computer program employed was based on the Profile Network Prediction Heidelberg method (PHD version 5.94−317; Heidelberg). This program consist of a neural network approach that averages several independently trained networks before making the final assessment with an average for successful prediction above 72%.[32]

4. Results and Discussion

Secondary Structure and Hydrophobic Moment. The secondary structure predictions using the Profile Network Prediction Heidelberg program are presented in Figure 1 for the carboxyl-end region of APO E3 and for the full length of APO AII, APO CIII, and APO AI. We only studied the secondary structure of the carboxyl-end region of APO E3, because the three-dimensional structure of its amino end region (residues 1−191) has been crystallographically solved.[33] According to the results shown in Figure 1 and Table 1, three

TABLE 1: Comparison between μH Values for the Different Regions Predicted as Amphipathic α Helices in Four Exchangeable Apolipoproteins

protein	number of residues in full protein	molecular weight (Da)	protein region	μH/ region
C terminal region of APO E3	299	34 200	204−221	0.28
			223−263	0.22
			266−287	0.42
APO AII	77	8708	7−27	0.49
			32−67	0.34
APO CIII	79	8760	7−41	0.21
			46−57	0.43
APO AI	243	28 300	9−47	0.28
			52−63	0.35
			69−163	0.27
			168−182	0.18
			189−240	0.28

α-helices are present in the carboxyl-end region of APO E3, encompassing residues 204−221, 223−263, and 266−287. In the case of APO AII, the predicted α-helical segments include residues 7−27 and 32−67. APO CIII presents two amphipathic α-helices that include residues 7−41 and 46−57. APO AI shows five sequences compatible with an amphipathic α-helices practically covering the whole molecule and including residues 9−47, 52−63, 69−163, 168−182, and 189−240. The amphipathic α-helical regions of the four apolipoproteins studied are shown in Figure 2 according to the helical wheel representation. It is clearly observed the typical asymmetrical distribution of nonpolar and polar amino acid residues in the different segments shown.

An estimation of the hydrophobic moment[34,35] for the amphipathic α-helices of the APOs AII, CIII, E3, and AI was made with the PCGene Program (IntelliGenetics Inc., 1991) using the following expression:

$$\mu H = \frac{1}{N}\sqrt{\left[\sum_{n=1}^{N} H_n \sin(\delta n)\right]^2 + \left[\sum_{n=1}^{N} H_n \cos(\delta n)\right]^2}$$

Here, H_n is a theoretical value of the degree of partition of an amino acid between the surface and the interior of a globular protein, and δ corresponds to the angle formed between amino acid lateral chains of two adjacent residues with respect to the plane of the α-helix (for an ideal α-helix, $\delta = 100°$). α-helical regions with μH values higher than 0.2 kcal/mol per residue could be considered as good amphipathic α-helices.[36] According to our calculations, which are presented in Table 1, the α-helical motifs present in the C-terminal region of APO E3 correspond to good amphipathic α-helices, because $\mu H > 0.2$ kcal/mol per residue. The two α-helices of APO AII gave also μH values higher that 0.2 kcal/mol per residue, as well as those of APO CIII. The only α-helix segment that does not fulfill this situation is the region 168−182 of APO AI, with a μH value of 0.18 kcal/mol per residue.

Circular Dichroism. The far-ultraviolet CD spectra (pH = 8.0, 20 °C) for APOs AII, CIII, E3, and AI are presented in Figure 3a. These experiments were made before the preparation of the monolayers to ensure protein integrity. We observed two minimum spectra values. The first one is around 222 nm, which corresponds to α-helix $n-\pi$ transitions. The second one is around *208* nm, which corresponds to both α-helix $\pi-\pi^*$ and random coil $\pi-\pi^*$ transitions. In all cases, the mean molar ellipticity at 222 nm ($[\theta]_{222}$) was independent of protein concentration through the range of 100−200 μg/mL. APOs secondary structure is well maintained when the proteins are dispersed in high concentrated KCl solutions. This fact will be used later in the monolayer experiments described below. Figure 3b shows the CD spectra of these proteins when dispersed into a buffered (pH = 8.0) 3.5 M KCl solution. These dispersions, notwithstanding to be in a transient state, lasted enough time to make the CD experiments. These experiments support the fact that the amphiphatic character of the APOs is preserved when they were deposited at the air−water surface of a highly concentrated KCl subphase.

To correlate protein stability and secondary structure content, a series of thermal denaturation experiments were carried out. As it is shown in Figures 4−7, APOs AII, CIII, E3, and AI, show a broad unfolding transition. In addition, all apolipoproteins showed a reversible heat unfolding character. Heating was performed from 20 to 90 °C followed by a reequilibration period at 20 °C, where the native structure was recovered (data not shown). Figures 4−7 show five independent curves for each heating condition. Because these curves are completely superimposable, the equilibrium character of the unfolding transition within the heat unfolding process is demonstrated.[37] Furthermore, the family of spectra recorded at several temperatures from 20 °C to 90 °C showed a well-defined isochromatic point at 204−205 nm for all of the APOs tested. In each case, the presence of an isochromatic point strongly suggests a two-state character. These results also showed that preservation of the α-helix structure is temperature dependent and its stabilization is enthalpy-driven.[37] The heat unfolding curves found at 208 and 222 nm for APO AII and APO CIII during thermal denaturation show two transition states (inset Figures 4 and 5). Moreover, the heat unfolding behavior of APO AII and APO CIII found at 222 nm suggests low cooperativity. In contrast, APO AI apparently presents only one transition state, because thermal denaturation curves found at 208 and 222 nm present a sigmoidal shape (inset Figure 6). According to our results, it is not clear if the unfolding process observed for APO E3 involves two or three states (inset Figure 7). However, in previous studies investigating APO E3 stability under chemical denaturation conditions, it was proposed the existence of two structural domains and the presence of stable intermediate states.[38]

Isotherms and BAM Observations. Although apolipoproteins can be solublilized in water, they remain at the interface when spread directly onto a 3.5 M KCl subphase solution, so they behave as Langmuir monolayers. Below, we present several monolayer stability tests supporting this fact for the APOs studied here. It was recently confirmed that human APO CI shares this behavior.[9] Although, we do not have a direct experimental confirmation about the stability of the α helices of the apolipoproteins studied here at the surface of the 3.5 M KCl subphase, the CD experiments reveal that their α helices content is well preserved, when they are dispersed in concentrated KCl solutions. In addition, grazing incidence X-ray diffraction experiments for the APO CI monolayer have recently confirmed that α helices remain stable at high lateral pressures, on this 3.5 M KCl subphase.[10]

Figure 8 shows typical isotherms for the apolipoproteins studied here, at pH = 8.0 and 25 °C. Several features are clearly recognized in these isotherms:

(a) A region of $\Pi \sim 0$ mN/m, starting at a very low surface area density, whose ending is in the range of $a = 5000$ Å^2/molec. for APO AII, $a = 2500$ Å^2/molec. for APO CIII, $a = 12\,000$ Å^2/molec. for APO AI, and $a = 10\,500$ Å^2/molec. for APO E3 when the number of molecules in the monolayer is ca. 3.83×10^{14}. This behavior is reminiscent of a gas/

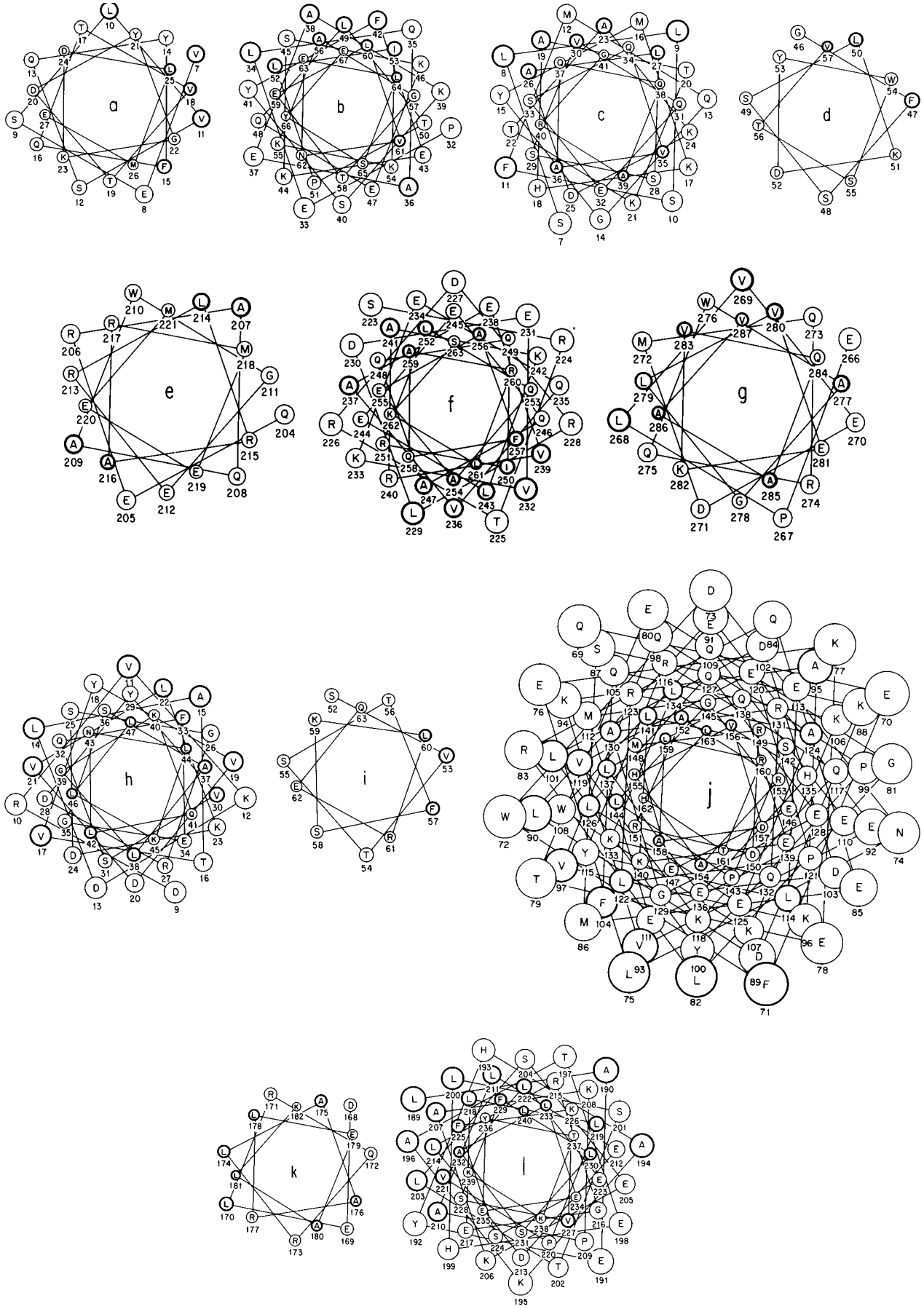

Figure 2. Helical wheel projections of amphipathic α helices present in Apo AII (a and b), APO CIII (c and d), APO E3 (e−g), and APO AI (h−l). Hydrophobic amino acid residues are circled with a thick line.

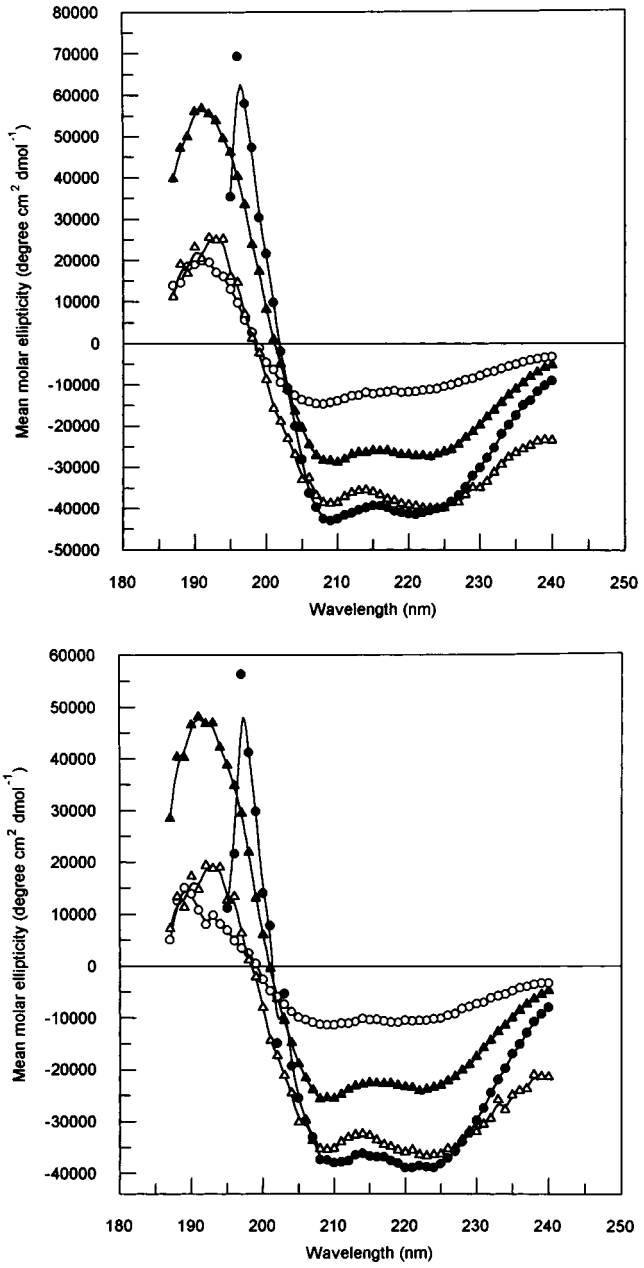

Figure 3. (a) Far-ultraviolet circular dichroism of APO AII (●), APO CIII (○), APO E3 (△), and APO AI (▲) in the phosphate buffered solution at 20 °C. (b) Far-ultraviolet circular dichroism of APO AII (●), APO CIII (○), APO E3 (△), and APO AI (▲) in the same buffered solution as in (a) containing 3.5 KCL at 20 °C.

condensed phase transition, although it was not possible to observe domains of condensed phase with the BAM. Nevertheless, for the case of APO E3 at very low densities ca. 100 000 Å^2/molec., we can observe black circular areas corresponding to gas-phase surrounded by bright condensed areas. At the ending of the coexistence in all protein monolayers, when the lateral pressure starts to increase, there is a tenuous and continuous change in the reflectivity because of a more condensed phase.

(b) Afterward, there is an important increase in lateral pressure, typical of a low compressibility condensed phase (L_1). Nevertheless, BAM observations did not allow us to see any well-defined domains. However, we could see defects in the monolayer and the way these defects move with a slower pace than similar defects in the gas/condensed phase coexistence. This fact reveals different viscosities in both phases.

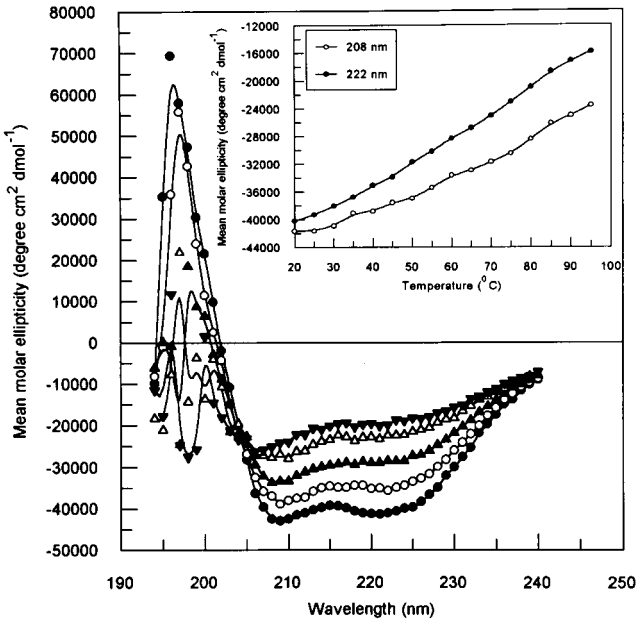

Figure 4. Temperature denaturation of APO AII studied by far-ultraviolet circular dichroism. Comparison of CD spectral characteristics at 20 (●), 40 (○), 60 (▲), 80 (△), and 90 °C (▼). Inset: mean molar ellipticity as a function of temperature taken at 208 and 222 nm

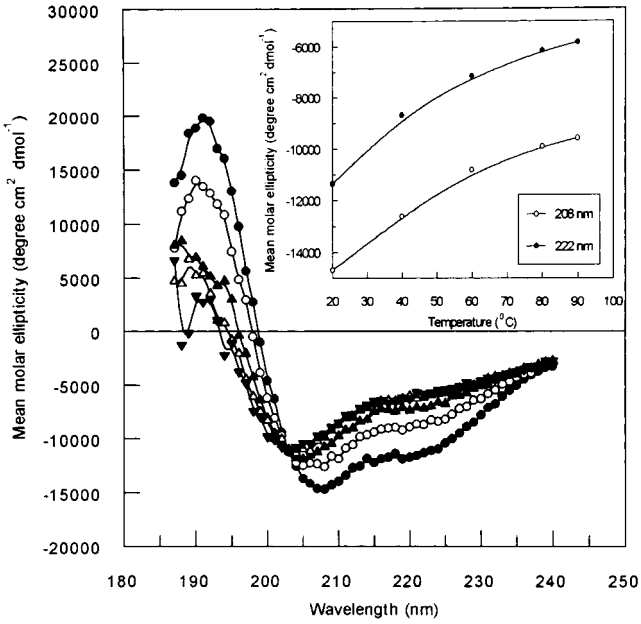

Figure 5. Thermal denaturation of APO CIII studied by far-ultraviolet circular dichroism. Comparison of CD spectral characteristics at 20 (●), 40 (○), 60 (▲), 80 (△), and 90 °C (▼). Inset: mean molar ellipticity as a function of temperature taken at 208 and 222 nm.

(c) After this point, the different proteins tested behave in a dissimilar way, because as pressure increases, APO AII and APO AI present, as described below, a second phase transition before the collapse. In the case of APO CIII, as soon as pressure increases, the monolayer collapses. This collapse takes place at $\Pi \sim 32$ mN/m, and it is confirmed with BAM observations (Figure 9). Here, many defects and mountain shaped structures typical of a collapse appear in the monolayer. However, in the case of APO E3, at the end of the compression, this apolipoprotein does not show a collapse, neither in the isotherms nor in BAM observations. We noticed that increasing the number of molecules in the monolayer above ca. 4×10^{14} the gas condensed phase transition end moves to higher area densities

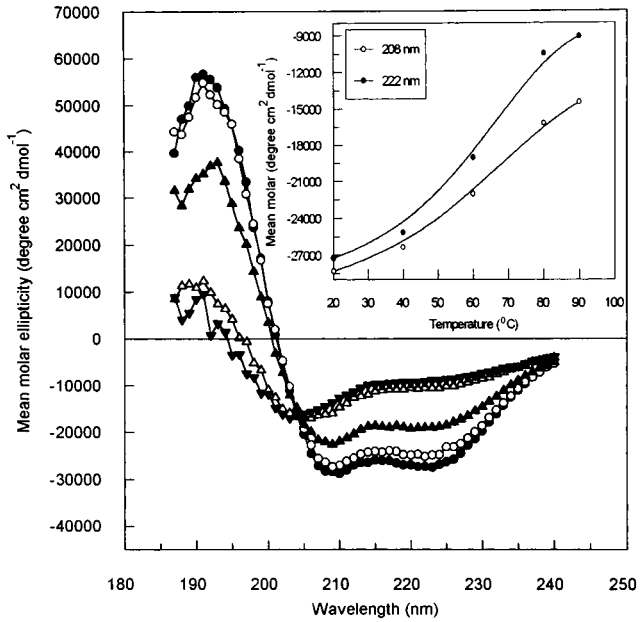

Figure 6. Thermal denaturation of APO AI studied by far-ultraviolet circular dichroism. Comparison of CD spectral characteristics at 20 (●), 40 (○), 60 (▲), 80 (△), and 90 °C (▼). Inset: mean molar ellipticity as a function of temperature taken at 208 and 222 nm.

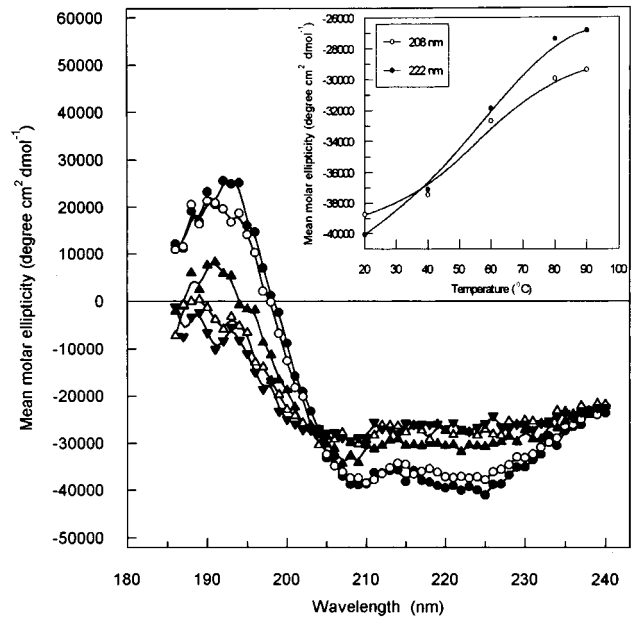

Figure 7. Thermal denaturation of APO E3 studied by far-ultraviolet circular dichroism. Comparison of CD spectral characteristics at 20 (●), 40 (○), 60 (▲), 80 (△), and 90 °C (▼). Inset: mean molar ellipticity as a function of temperature taken at 208 and 222 nm.

(Figure 8b). One possibility for this behavior could be explained through protein solubilization in the subphase as soon as lateral pressure increases, similar to what has been observed in Gibbs monolayers. However, this seems not to be the case, because a monolayer of APO E3 with 8.75×10^{14} molecules left for more than 1 h at a lateral pressure of 33.7 mN/m presented a loss in lateral pressure of only 6 mN/m., for that elapsed time. Therefore, the rate of lateral pressure loss is negligible for the current compression times ($\sim^1/_2$ h). Also, at this concentration of proteins in the monolayer, we ran cycles of compression (up to $\Pi \sim 40$ mN/m), expansion (down to $\Pi \sim 0$ mN/m), and further recompression (up to $\Pi \sim 40$ mN/m). Because it is common in monolayers, the expansion does not retrace the

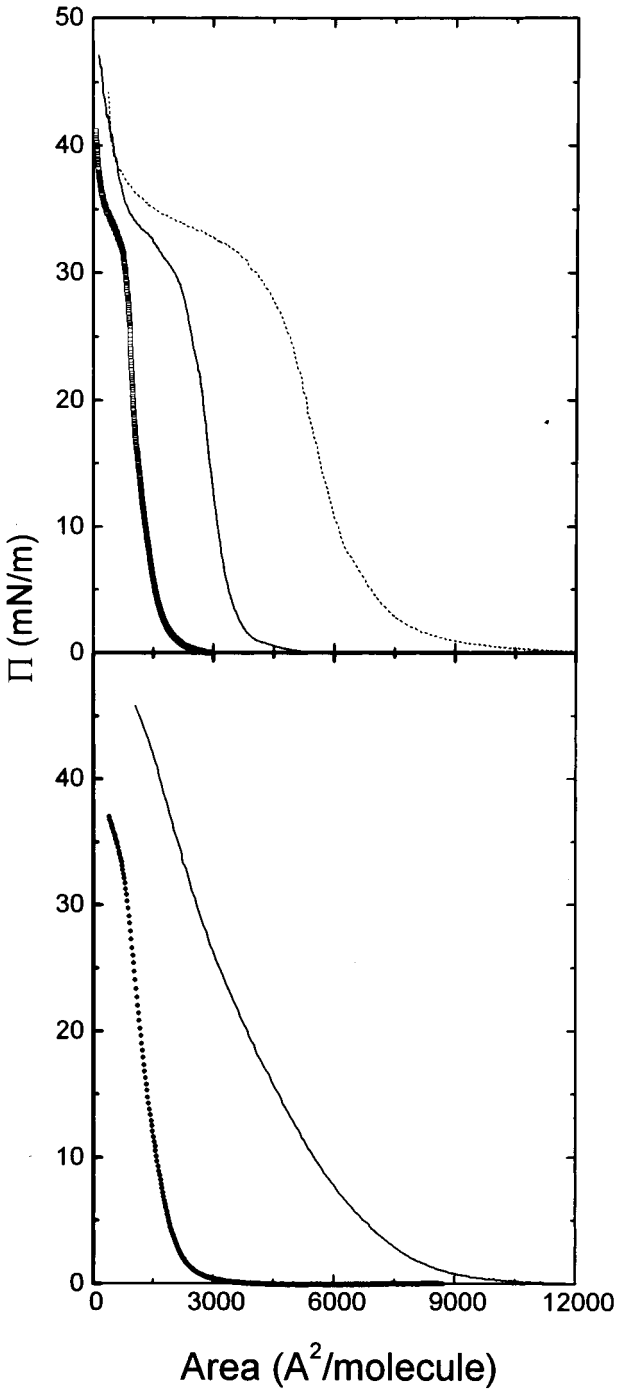

Figure 8. Typical isotherms for the different Apolipoproteins studied here at 25 °C. Upper panel: isotherms of APO AII (−), APO CIII (□), and APO AI (- -). Lower panel: isotherms for APO E3 obtained by depositing different quantities of protein. 3.8×10^{14} (−) and 11.5×10^{14} molecules (●).

compression isotherm but the next compression presented the same characteristics of the first compression, although some area is lost. These results are probably indicating that the protein monolayer is becoming organized in some way and not being solubilized in the subphase. Because, this protein presents a more complex tertiary structure than the other proteins studied here, it is not surprising that APO E3 might be more prone to molecular rearrangements.

As mentioned above, APO AII and APO AI present a second phase transition before the collapse. In the case of APO AII, when the condensed phase L_1 is compressed, we find a wide kink at $\Pi \sim 30-35$ mN/m and $a \sim 1000-2500$ Å^2/molec.,

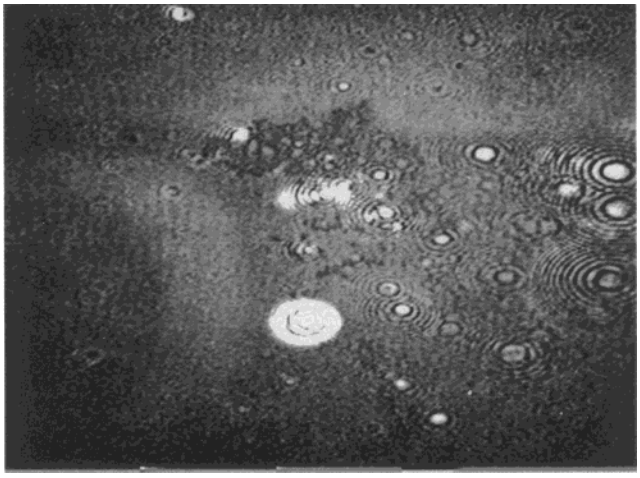

Figure 9. APO CIII collapsed monolayer at $\Pi \sim 41$ mN/m and $a \sim 200$ Å^2/molec. as observed with BAM.

typical of a phase transition between two condensed phases (L_1/L_2). BAM observations (Figure 10a,b) revealed that the monolayer changed from a tenuous gray to a bright gray. The bright areas are quite big domains, covering the entire field of view, without the presence of domains of different shades of gray. This phase transition is reversible, because cycles of compression and decompression show how the new phase appears at $\Pi \sim 35$ mN/m, but with hysteresis. These observations seem to indicate that the L_1/L_2 phase transition in APO AII is a first-order transition. At lateral pressures of the order of $\Pi \sim 22$ mN/m, there is always a small change of slope in the isotherms, but we could not confirm if this corresponds to a phase transition. In the case of APO AI, at $\Pi \sim 30$ mN/m and $a \sim 4500$ Å^2/molec, there is a change in the slope of the isotherm. However, domains appear in the BAM images until the lateral pressure reaches $\Pi \sim 35$ mN/m (see Figure 11). The domains are big bright stripes without any shade of gray. They seem to be rigid, and in some cases, it is easy to observe with the BAM how the other phase, which is more fluid, flows between the big bright domains. We made compression and expansion cycles around the transition pressure. The domains appeared and disappeared as we were above or below $\Pi \sim 35$ mN/m., respectively. Because the transition showed hysteresis, it seems to be a first-order phase transition. At the end of the compression, the APO AII monolayer collapses at $\Pi \sim 47$ mN/m and $a \sim 500$ Å^2/molec. (Figure 10c). In the same way, when the APO AI monolayer reaches $\Pi \sim 41$ mN/m and $a \sim 500$ Å^2/molec., it also collapses. Many defects (interference rings) as well as mountain shaped structures typical of collapse do appear in the BAM images.

To find out the stability of APO AII and APO AI monolayers on the air/water interface, we left monolayers at $\Pi \sim 30$ mN/m for an hour. The decrease in lateral pressure observed was in the order of 3 mN/m. We also ran cycles of compression (up to $\Pi \sim 44$ mN/m for APO AII and 39 mN/m for APO AI), expansion (down to $\Pi \sim 0$ mN/m), and further recompression (up to $\Pi \sim 45$ mN/ for APO AII and 40 mN/m for APO AI m). The expansion does not retrace the compression isotherm, but the next recompression presented the same characteristics of the first compression, although some area is lost (BAM images reveal more defects). All of these experiments and the reversibility of the L_1/L_2 phase transition mentioned above seem to indicate that if protein is lost from the surface, when an isotherm is made, it must be at a negligible rate compared to the velocity of the compression.

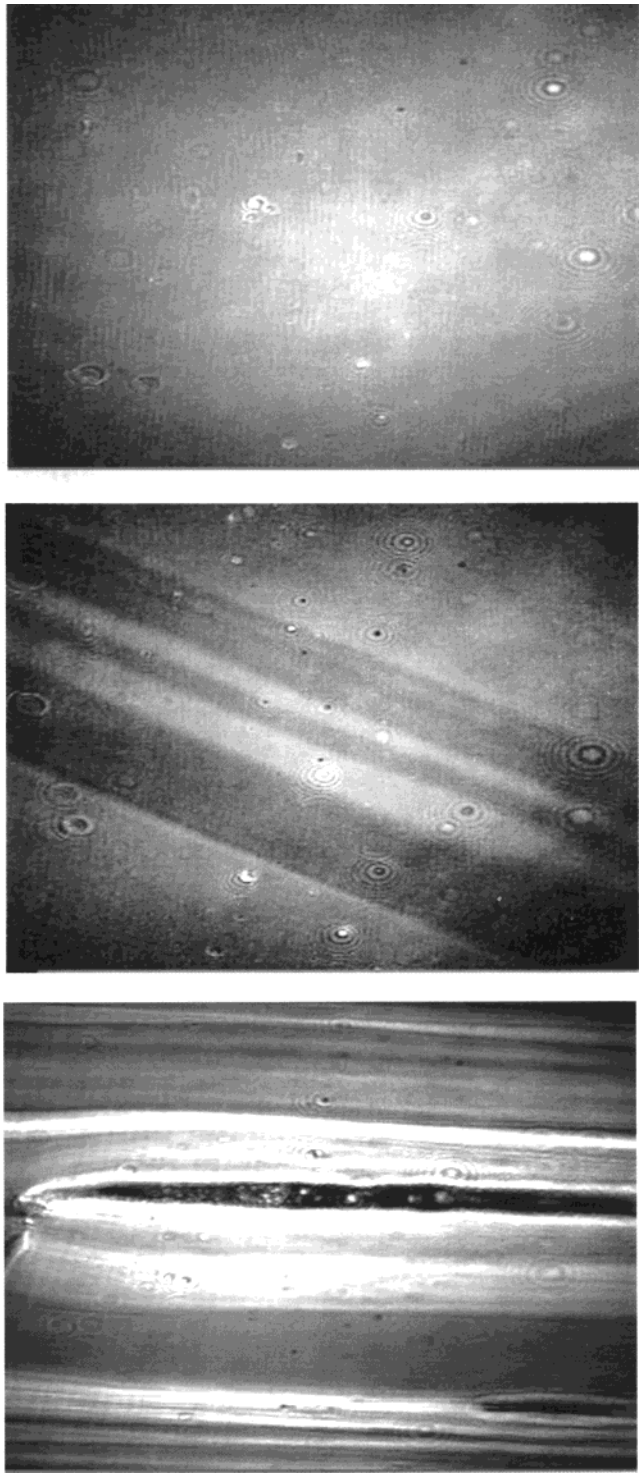

Figure 10. BAM images of APO AII protein monolayer. (a) Just before the L_1/L_2 transition, (b) at the L_1/L_2 coexistence, $\Pi \sim 30-35$ and $a \sim 1000-2000$ Å^2/molec., and (c) Collapsed monolayer $\Pi \sim 47$ mN/m and $a \sim 500$ Å^2/molec.

We also prepared monolayers made of APO AII over subphases at pH = 7.0. The phase transition sequence was the same as that found at pH = 8.0, except that the second transition does occur at $\Pi \sim 32-37$ mN/m and between 900 and 2900 Å^2/molec. Here, the isotherm is more horizontal than in the case of pH = 8.0 (data not shown). The small change of slope mentioned at pH = 8.0 ($\Pi \sim 22$ mN/m) also appeared but in a more pronounced way.

We made grazing incidence X-ray diffraction experiments for the APO CIII monolayer in the L_1 phase at $\Pi \sim 30$ mN/m,

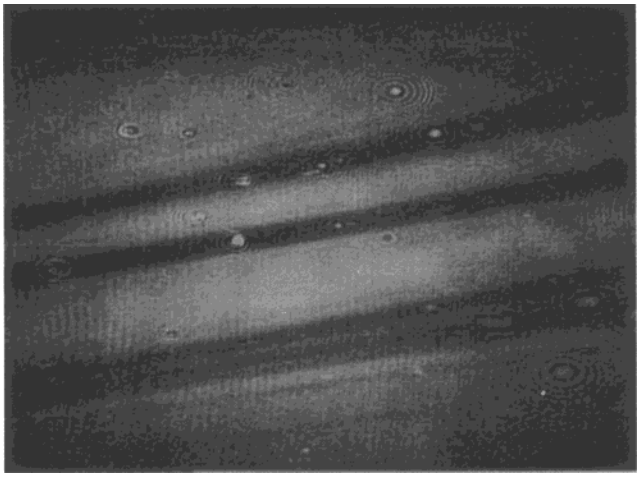

Figure 11. BAM image of the APO AI monolayer at the L_1/L_2 coexistence, $\Pi \sim 35$ mN/m and $a \sim 1500$ Å^2/molec.

as well, for the APO AI monolayer at two lateral pressures, $\Pi \sim 29$ and 35 mN/m (BW1 beam line at the Hasylab synchrotron facility, using an intense X-ray beam of a wavelength of $\lambda = 1.303$ Å, foot print ~ 10 cm^2, $\theta \sim 0.12°$). The contours of equal intensity vs the in-plane and out-of-plane scattering vectors components K_{xy} and K_z revealed no peaks in all of the experiments. Therefore, the L_1 phase of the APO CIII ($\Pi \sim 30$ mN/m) and of APO AI ($\Pi \sim 29$ mN/m), correspond to a liquid phase, because there is no ordering. For the case of APO AI, at $\Pi \sim 35$ mN/m, all seems to indicate that the denser phase is a disordered phase.

On the basis of our results, it is reasonable to model the studied APOs as amphiphilic α helices bonded by loose hinges. These proteins would be traveling on a landscape of close energy minimum configurations, when deposited onto a water subphase, which is also working as a thermal reservoir. The different protein configurations must have the restriction of being laying horizontally on the subphase, because of the amphiphilic character of these proteins, as discussed above. At low surface areas, two phases are coexisting, the gas and the liquid phase. BAM observations showed that, in both phases, there is only one kind of shade. There are no monolayer domains revealing some molecular order, which could give rise to different textures, i.e., they are disordered phases.

The second phase transition in the monolayers of APO AI and AII probably is similar to the phase transition between condensed phases of the monolayer of APO CI,[9] where proteins desorb one of its amphiphilic α-helical segments from the surface, to occupy less surface area. This conformational change could explain the area loss and the high reflectivity difference between the phases. In addition, the desorbed α helices probably are not correlated either intra- or supra-molecularly, because different textures are not observed in the domains of the condensed phases. The amphiphilic α-helical segment going out from the surface must be that with the lowest μH value and short size. In such a case, the L_1/L_2 transition seems to be of first-order, because of the large change of area per molecule. After the conformational change, protein molecules are considerably close to each other, surely increasing the attractive contribution to the free energy. Therefore, the transition must be governed primarily by the interplay between the conformational and the attractive contributions to the free energy. Grazing incidence X-ray diffraction experiments, as well as, atomic force microscopy studies on transferred monolayers are necessary to give a better understanding of this transition. These studies are underway.

The presence of amphipathic α helices might be considered a key factor in defining the physiological behavior of exchangeable apolipoproteins. We are certain that these kinds of studies will contribute to give a clearer picture of the mechanisms that facilitate the exchange of these proteins between lipoproteins and between lipoproteins and membranes as well as the structural changes related to their physiological function

Acknowledgment. We thank the help of J. Ruiz-García and G. Brezesinski for running the X-ray diffraction experiments as well as the beam time at Hasylab in DESY (Hamburg, Germany). This study has been partially supported by CONACYT and DGAPA-UNAM (Grants: MB072, 27513E, IN-212094, and IN-103598).

References and Notes

(1) Kaganer, V. M.; Möhwald, H.; Dutta, P. *Rev. Mod. Phys*. **1999**, *71*, 779.

(2) Tanaka, H.; Akatsuka, T.; Murakami, T.; Ogoma, Y.; Abe, K.; Kondo, Y. *J. Biochem*. **1997**, *121*, 206.

(3) Tanaka, H.; Akatsuka, T.; Ohe, T.; Ogoma, Y.; Abe, K.; Kondo, Y. *Polym. Adv. Technol*. **1998**, *9*, 150.

(4) Tanaka, H.; Hayashi, K.; Akatsuka, T.; Murakami, T.; Toyama, J.; Noda, K.; Kida, T.; Ogoma, Y.; Fujii, T.; Kondo, Y. *J. Biochem*. **1995**, *117*, 1151.

(5) Dziri, L.; Boussaad, S.; Wang, S.; Leblanc, R. M. *J. Phys. Chem. B*. **1997**, *101*, 6741.

(6) Frey, W.; Schief, W. R.; Vogel, V. *Langmuir* **1996**, *12*, 1312.

(7) Lipp, M.; Lee, K. Y. C.; Waring, A.; Zasadzinki, J. A. *Biophys. J*. **1997**, *72*, 2783.

(8) Chen, X.; Moser, C. C.; Pillud, D. L.; Dutton, P. L. *J. Phys. Chem. B*. 1998, *102*, 6424.

(9) Bolaños-García, V. M.; Mas-Oliva, J.; Ramos, S.; Castillo, R. *J. Phys. Chem. B* **1999**, *103*, 6236.

(10) Ruiz-García, J.; Moreno, A.; Brezesinski, G.; Möhwald, H.; Mas-Oliva, J.; Castillo, R. To be published.

(11) Xicohtencatl-Cortes, J.; Moreno, A.; Mas-Oliva, J.; Castillo, R. To be published.

(12) Gotto, A. M. H.; Pownall, J.; Havel, R. J. *Methods Enzymol*. **1986**, *128*, 3.

(13) Schonfeld, G.; Patsch, W.; Rudel, L. L.; Nelson, C.; Epstein, M.; Olson, R. E. *J. Clin. Invest.* **1982**, *69*, 1072.

(14) Hussain, M. M.; Zannis, V. I. *Biochemsitry* **1990**, *29*, 209.

(15) López, J.; Latta, M.; Collet, X.; Vanloo, B.; Jung, G.; Denefle, P.; Rosseneu, M.; Chambaz, J. *Eur. J. Biochem.* **1994**, *225*, 1141.

(16) Lusis, A. J. *J. Lipid Res.* **1988**, *29*, 397.

(17) Doolittle, M. H.; LeBoeuf, R. C.; Warden, C. H.; Bee, L. M.; Lusis, A. J. *J. Biol. Chem.* **1990**, *265*, 16380.

(18) Lagocki, P. A.; Scanu, A. M. *J. Biol. Chem.* **1980**, *255*, 3701.

(19) Havel, R.; Kane, J. P. In *The Metabolic and Molecular Bases of Inherited Disease*; Scriver, C. R., Beaudet, A. L., Sly, W. S., Valle, E. L., Eds.; McGraw-Hill: New York, 1995; p 1841.

(20) Quarfordt, S. H.; Michalopoulos, G.; Schirme, B. *J. Biol Chem.* **1982**, *257*, 14642.

(21) Windler, E.; Havel, R. J. *J. Lipid Res.* **1986**, *26*, 556.

(22) Mahley, R. W.; Weisgraber, K. H.; Farese, R. V. In *Williams Textbook of Endocrinology*, 9th ed.; Wilson, J. D., Foster, D. W., Kronenberg, H. M., Larsen, P. R., Eds.; W. B. Saunders: Philadelphia, PA, 1998; p 1099.

(23) Mahley, R. W. *Science* **1988**, *240*, 622.

(24) Scanu, A. M. *Lipids* **1978**, *13*, 920.

(25) Schultz, J. R.; Verstuyft, J. G.; Gong, E. L.; Nichols, A. V.; Rubin. E. M. *Nature* **1993**, *365*, 762.

(26) Warden, C. H.; Hedrick, C. C.; Qiao, J. H.; Castellani, L. W.; Lusis, A. J. *Science* **1993**, *261*, 469.

(27) Plumb, A. S.; Scott, C. J.; Breslow, J. L. *Proc. Natl. Acad. Sci. U.S.A.* **1994**, *91*, 9607.

(28) Fielding, C. J.; Shore, V. G.; Fielding, P. E. *Biochem. Biophys. Res. Commun.* **1972**, *46*, 1493.

(29) Yokoyama, S.; Fukushima, D.; Kupferberg, J. P.; Kezdy, F. J.; Kaiser, E. T. *J. Biol. Chem.* **1980**, *255*, 7333.

(30) Acton, S.; Rigotti, A.; Landschulz, K. T.; Xu, S.; Hobbs, H. H.; Krieger, M. *Science* **1996**, *271*, 518.
(31) Pace, C. N.; Vajdos, F.; Fee, L.; Grimsley, G.; Gray, T. *Protein Sci.* **1995**, *4*, 2411.
(32) Rost, B.; Sander, C. *Proteins* **1994**, *19*, 55.
(33) Wilson, C.; Wardell, M. R.; Weisgraber, K. H.; Mahley, R. W.; Agard, D. A. *Science* **1991**, *252*, 1817.
(34) Eisenberg, D.; Weiss, R. M.; Terwilliger, T. C. *Nature* **1982**, *299*, 371.
(35) Eisenberg, D.; Robert, M. W.; Thomas, T. C. *Proc. Natl. Acad. Sci. U.S.A.* **1984**, *81*, 140.
(36) Rozek, A.; Buchko, G. W.; Kanda, P.; Cushley, R. J. *Protein Sci.* **1997**, *6*, 1858.
(37) Fersht, A. Practical Methods for Kinetics Equilibria. *Structure and Mechanism in Protein Science*; W. H. Freeman and Company: New York, 1999; Chapter 6, p 191.
(38) Wetterau, J. R.; Aggerbeck, P.; Rall, S. C.; Weisgraber, K. H. *J. Biol. Chem.* **1988**, *263*, 6240.